

Article

Historical Trends and Characteristics of Meteorological Drought Based on Standardized Precipitation Index and Standardized Precipitation Evapotranspiration Index over the Past 70 Years in China (1951–2020)

Jiwei Sun ^{1,*}, Shuoben Bi ^{1,*}, Bashar Bashir ², Zhangxi Ge ³, Kexin Wu ³, Abdullah Alsalman ², Brian Odhiambo Ayugi ⁴ and Karam Alsafadi ^{5,*}

¹ School of Geographical Sciences, Nanjing University of Information Science and Technology, Nanjing 210044, China

² Department of Civil Engineering, College of Engineering, King Saud University, P.O. Box 800, Riyadh 11421, Saudi Arabia

³ School of Management Engineering, Nanjing University of Information Science and Technology, Nanjing 210044, China

⁴ Department of Civil Engineering, Seoul National University of Science and Technology, Seoul 01811, Republic of Korea

⁵ School of Environmental Science and Engineering, Nanjing University of Information Science and Technology, Nanjing 210044, China

* Correspondence: bishuoben@163.com (S.B.); karam.alsafadi@alexu.edu.eg or 200040@nuist.edu.cn (K.A.)



check for updates

Citation: Sun, J.; Bi, S.; Bashir, B.; Ge, Z.; Wu, K.; Alsalman, A.; Ayugi, B.O.; Alsafadi, K. Historical Trends and Characteristics of Meteorological Drought Based on Standardized Precipitation Index and Standardized Precipitation Evapotranspiration Index over the Past 70 Years in China (1951–2020). *Sustainability* **2023**, *15*, 10875. <https://doi.org/10.3390/su151410875>

Academic Editor: Chengpeng Lu

Received: 10 June 2023

Revised: 2 July 2023

Accepted: 9 July 2023

Published: 11 July 2023



Copyright: © 2023 by the authors. Licensee MDPI, Basel, Switzerland. This article is an open access article distributed under the terms and conditions of the Creative Commons Attribution (CC BY) license (<https://creativecommons.org/licenses/by/4.0/>).

Abstract: Against the backdrop of global climate change, the frequency of drought events is increasing, leading to significant impacts on human society and development. Therefore, it is crucial to study the propagation patterns and trends of drought characteristics over a long timescale. The main objective of this study is to delineate the dynamics of drought characteristics by examining their propagation patterns in China from 1951 to 2020. In this study, precipitation data from meteorological stations across mainland China were used. A comprehensive dataset consisting of 700 stations over the past 70 years was collected and analyzed. To ensure data accuracy, the GPCC (the Global Precipitation Climatology Center) database was employed for data correction and gap-filling. Long-term drought evolution was assessed using both the SPI-12 (standardized precipitation index) and SPEI-12 (standardized precipitation evapotranspiration index) to detect drought characteristics. Two Moran indices were applied to identify propagation patterns, and the MK (the Mann–Kendall) analysis method, along with the Theil–Sen slope estimator, was utilized to track historical trends of these indices. The findings of this study reveal the following key results: (i) Based on the SPI-12, the main areas of China that are prone to drought are mostly concentrated around the Hu Huanyong Line, indicating a tendency towards drying based on the decadal change analysis. (ii) The distribution of drought-prone areas in China, as indicated by the SPEI-12, is extensive and widely distributed, with a correlation to urbanization and population density. These drought-prone areas are gradually expanding. (iii) Between 2010 and 2011, China experienced the most severe drought event in nearly 70 years, affecting nearly 50% of the country’s area with a high degree of severity. This event may be attributed to atmospheric circulation variability, exacerbated by the impact of urbanization on precipitation and drought. (iv) The frequency of drought occurrence in China gradually decreases from south to north, with the northeast and northern regions being less affected. However, areas with less frequent droughts experience longer and more severe drought durations. In conclusion, this study provides valuable insights into the characteristics and propagation patterns of drought in China, offering essential information for the development of effective strategies to mitigate the impacts of drought events.

Keywords: drought; Moran’s I Index; Mann–Kendall test; urban droughts; standardized precipitation evapotranspiration index; drought characterization; evapotranspiration; GPCC

1. Introduction

Due to the impact of climate change, the uneven spatial distribution of water resources across different regions of the world has become increasingly severe in recent decades [1,2]. This is primarily due to recurrent episodes of frequent drought events, which have a devastating impact on regional ecosystems and human social development [3]. It is important to note that rising temperatures and declining precipitation exacerbate the severity and duration of droughts [4,5]. Throughout history, China has experienced recurring droughts that have caused significant damage to the economy and agriculture [6]. Alarming, over the past 50 years, the agricultural damage rate caused by drought in China has increased by approximately 0.5% per decade [7]. Moreover, some studies suggest that this trend may continue until 2100 [8]. A severe drought event that occurred in China between 2009 and 2010 resulted in substantial economic losses amounting to nearly 46.53 billion CNY Yuan [9]. Additionally, it left approximately 16 million people and 11 million livestock without access to adequate drinking water [10–12]. Future climate projections indicate that droughts are expected to become more severe, prolonged, and frequent [13–16]. Consequently, it is crucial to develop a comprehensive understanding of drought characteristics. Such understanding will aid in monitoring and predicting drought events, facilitating the formulation of effective strategies to mitigate the hazards associated with drought. However, to mitigate the potential worst-case scenario of drought effects, there is an urgent need to delineate the characteristics of drought and its propagation patterns across China, ensuring long-term sustainability.

Currently, existing studies relating to drought characteristics have been conducted in China in order to understand its propagation patterns [17]. For instance, recent studies have reported that the duration of extreme summer droughts in northern China has been prolonged [18,19]. In another related study, Zhang et al. [20] reported a noteworthy trend in drought along the northern parts of Xinjiang, while declining patterns in the southern and eastern regions. The observed trends in drought in northwest China in the last 30 years have shown a marked trend towards wetting [21]. Meanwhile, projected tendencies show that there may be an increase in drought occurrence in southern China [22], as a result of the changes in dynamic and thermodynamic features that influence precipitation patterns [23,24]. To detect and characterize drought, many drought indices have been developed and used to assess drought effects. These include the Standardized Precipitation Index (SPI) [25], the Standardized Precipitation Evapotranspiration Index (SPEI) [26], the Palmer Drought Severity Index (PDSI) [27], the Soil Moisture Deficit Index (SMDI) and Evapotranspiration Deficit Index (ETDI) [28], the Standardized Wetness Index (SWI) [29], and the Evapotranspiration Deficit-Based Drought Index (SDEI) [30]. The SPI and SPEI have been widely used in drought research around the world, such as in South Africa [31], Zambia [32], China [33], Turkey [34], North Korea [35], Moldova [36], Syria [37], and Nepal [38]. Different types of droughts, including meteorological, agricultural, hydrological, and socio-economic, have been analyzed.

Previous studies have shown that using SPI and SPEI to assess drought conditions has been particularly effective [33,39,40]. However, it has been observed that the SPEI detects more severe drought events compared to the SPI [33]. Nevertheless, there have been limited studies that utilize long-term data over mainland China, employing SPI and SPEI at different timescales to examine drought characteristics, propagation patterns, and historical trends [41,42]. Since droughts usually affect large areas, it is crucial to determine whether the information on drought characteristics exhibits contrasting or interconnected spatial patterns based on meteorological stations. These stations can accurately reflect meteorological drought conditions compared to common gridded data. Therefore, a comprehensive assessment of the spatiotemporal dynamics of drought between the SPI and SPEI in mainland China is critical for understanding the impact of atmospheric water demand on drought in the context of climate change. This aspect has not been well covered in previous studies. Furthermore, as meteorological stations are often located within urban areas or in the surrounding regions of cities, it is vital to detect the evolution of

urban drought. This helps in understanding the influence of heat islands and atmospheric evaporative demand on the evolution of urban drought over a 70-year period.

In this study, we performed drought analysis using SPI and SPEI. SPI is a precipitation-based index, and SPEI is a novel and ideal index used to analyze the combined impact of precipitation and evapotranspiration on drought. Therefore, this study evaluated and compared the drought characteristics of the two indices and the importance of different stations for drought research to provide future drought researchers with some station selection options. The specific objectives include exploring the variability of climate variables, investigating the time and spatial variation characteristics of SPI and SPEI for quantifying drought, conducting Moran's I Index analysis to provide valuable insights into the characteristics and propagation patterns of drought in China, by analyzing the duration, severity, intensity, and peak of drought in large areas, and producing maps of drought duration, severity, intensity, and peak. Therefore, the main objective of this study is to evaluate the dynamic characteristics of drought in China over the past 70 years, with a focus on the following issues: (i) using the SPI/SPEI drought index to evaluate the spatiotemporal characteristics of drought in China from 1951 to 2020; (ii) the spatial distribution of severe droughts in China over the past 70 years; (iii) the spatial variation of the extreme drought event that occurred in China during 2010–2011; and (iv) pattern analysis of SPI and SPEI drought characteristics.

2. Materials and Methods

2.1. Study Area and Data Collection

China is situated in the eastern part of the Eurasian continent, spanning latitudes $3^{\circ}51' \text{ N}$ – $53^{\circ}33' \text{ N}$ and longitudes $73^{\circ}33' \text{ E}$ – $135^{\circ}5' \text{ E}$. It covers a land area of approximately 9.6 million km^2 (Figure 1). The country's eastern side is bordered by the Pacific Ocean, while its southwestern side is adjacent to the Qinghai–Tibet Plateau [43]. These diverse geographical features give rise to unique climate characteristics, which can be classified as monsoon climate and continental climate [44]. In China, precipitation is primarily concentrated in the summer season across most regions, while its distribution varies spatially. The eastern parts experience higher precipitation levels compared to the western areas, with a gradual decrease in precipitation from the southeast coast to the northwest inland. This pattern is attributed to the influence of winter monsoons, which are cold and dry, during the winter season, while summer monsoons from the ocean bring warmth, rain, and influence during summer. The vast eastern part of China is greatly affected by the southeast and southwest monsoons, leading to abundant precipitation. Conversely, the inland northwest is less influenced by the summer monsoon and receives sparse precipitation.

For this study, precipitation data from 1951 to 2016 were obtained from the China Meteorological data sharing service system at a monthly timescale (<http://data.cma.cn/en>, accessed on 28 February 2018). The data were sourced from 756 benchmark ground observation stations or automatic stations that covered most of the country. Due to the limited duration of observed data at certain stations, data from 52 stations were excluded. To address missing data, precipitation data at a monthly timescale from 1951 to 2020 were acquired from the Global Precipitation Climatology Center (GPCC; Schamm et al. [45]) (<http://gpcc.dwd.de/>, accessed on 24 February 2023). This dataset was used to correct and fill in the missing values, resulting in a final dataset spanning 1951–2020 with 700 stations that had valid data. It is worth mentioning that the data underwent a homogeneity test prior to their utilization in the analysis of drought indices. Additional information regarding the distribution of missing values and the correction and filling process is given in Appendix A (Figure A1), which indicates that the correlations between the GPCC data and observed precipitation are very high. On the other hand, evapotranspiration data from 1951 to 2020 were obtained from a global grid dataset of monthly climate data developed by the Climatic Research Unit (CRU TS v4.06) [46] at the University of East Anglia, UK (<https://crudata.uea.ac.uk/cru/data/hrg/>, accessed on 1 February 2023). The SPI/SPEI

values calculated over a 12-month period for the entire study area are represented as a two-dimensional array.

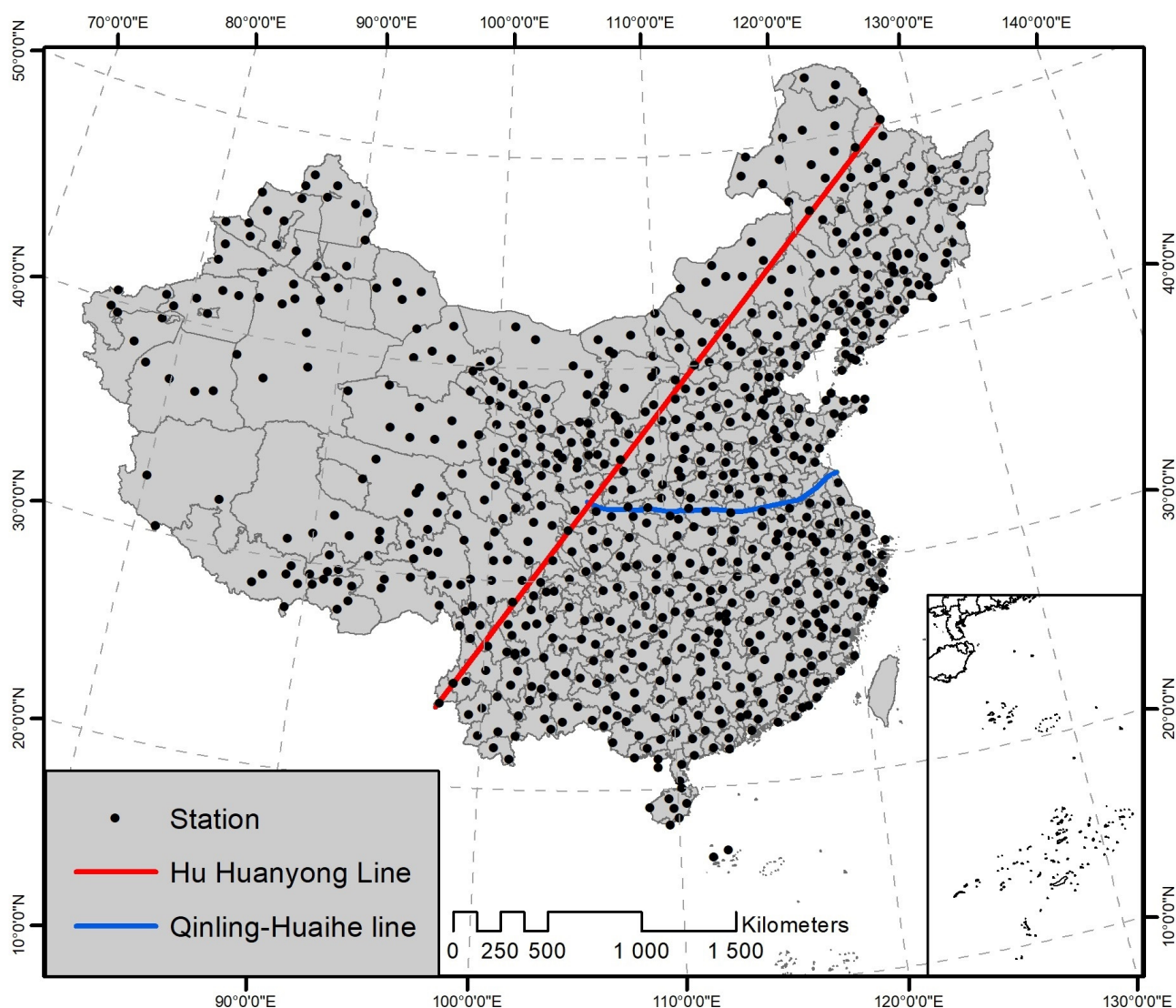


Figure 1. Study area location and distribution of stations.

2.2. Drought Indices

2.2.1. Standardized Precipitation Index (SPI)

The SPI is a precipitation-based index [25]. Since the distribution of precipitation is non-normal, the SPI first calculates the probability of the gamma (Γ) distribution of precipitation. Then, it normalizes the probability of its Γ distribution and uses the resulting standardized cumulative frequency distribution of precipitation for assessment and analysis, calculated as follows:

Assume that the amount of precipitation in a given time period is a random variable x , and when x is not 0 ($x > 0$), the probability density function of its gamma distribution is as follows:

$$f(x) = \frac{1}{\beta^\gamma \Gamma(\gamma)} x^{\gamma-1} e^{-\frac{x}{\beta}} \quad (1)$$

In the formula, γ and β are the shape function and scale parameter of the Γ distribution function, respectively, calculated using the maximum likelihood method.

$$\gamma = \frac{1 + \sqrt{1 + \frac{4A}{3}}}{4A} \quad (2)$$

$$\beta = \frac{\bar{x}}{4A} \quad (3)$$

$$A = \log_{10}(\bar{x}) - \frac{1}{n} \sum_{i=1}^n \log_{10} x_i \quad (4)$$

In the above equation, x_i is the sequence of precipitation data and \bar{x} is the climatic mean of precipitation. Thus, the amount of precipitation x_0 in a given year yields the probability that the random variable x is less than the x_0 event.

$$F(x < x_0) = \int_0^{x_0} f(x) dx \quad (5)$$

Assume that the precipitation during a specific time period is 0.

$$F(x = 0) = m/n \quad (6)$$

In the formula, m is the number of samples with 0 precipitation and n is the total number of samples. The probability that x takes 0 value.

$$\text{When } 0 < F(x) \leq 0.5, t = \sqrt{\ln \frac{1}{F^2}}$$

$$\text{SPEI} = \left(\frac{(c_2 t + c_1)t + c_0}{[(d_3 t + d_2)t + d_1]t + 1} \right) - t \quad (7)$$

$$\text{When } 0.5 < F(x) \leq 1.0, t = \sqrt{\ln \frac{1}{(1-F)^2}}$$

$$\text{SPEI} = t - \left(\frac{(c_2 t + c_1)t + c_0}{[(d_3 t + d_2)t + d_1]t + 1} \right) \quad (8)$$

In the above equation, $c_0 = 2.515517$, $c_1 = 0.802853$, $c_2 = 0.0110328$, $d_1 = 1.432788$, $d_2 = 0.189269$, and $d_3 = 0.001308$.

2.2.2. Standardized Precipitation Evapotranspiration Index (SPEI)

The main steps in calculating the SPEI [26] can be summarized as follows:

- Calculating the difference between potential evapotranspiration (PET) and monthly precipitation provides the monthly climatic water balance (D_i) as follows:

$$D_i = P_i - PET_i \quad (9)$$

P_i is monthly precipitation, and PET_i is the monthly potential evapotranspiration.

- A Log-logistic probability distribution with 3 parameters (scale function (α), shape function (β), and origin parameter (γ)) was used to linearly fit the D_i series to obtain the cumulative function of the probability distribution:

$$F(x) = \left[1 + \left(\frac{\alpha}{x - \gamma} \right)^\beta \right]^{-1} \quad (10)$$

- The cumulative probability density (P), subjected to standard normalization, is calculated as the value of the SPEI corresponding to each value in the series:

$$\text{SPEI} = w - \frac{c_0 + c_1w + c_2w^2}{1 + d_1w + d_2w^2 + d_3w^3} \quad (11)$$

$$w = \sqrt{-2\ln P} \quad (12)$$

If $P > 0.5$, then $P = 1 - F(x)$; if $P \leq 0.5$, then $P = F(x)$. The values of the remaining parameters are $c_0 = 2.515517$, $c_1 = 0.802853$, $c_2 = 0.0110328$, $d_1 = 1.432788$, $d_2 = 0.189269$, and $d_3 = 0.001308$.

The positive values indicate wet conditions, while the negative values indicate drought conditions. Interestingly, the SPEI is superior to the SPI in terms of drought characterization and climate change monitoring since the SPEI takes into consideration both temperatures (used to compute PET). Nevertheless, it is important to mention here that the data were obtained and computed at a 12-month timescale (i.e., SPEI-12 and SPI-12). Because the shorter the calculation time of the SPI/SPEI, the quicker the response to changes in precipitation, but the more sensitive it is to fluctuations in precipitation noise. Sometimes, when results are calculated using an SPI/SPEI of less than 12 months, false drought signals can be received, which are affected by short-term weather fluctuations. Results calculated using an SPI greater than 12 months have a response time that is too long and cannot promptly reflect short-term drought conditions, which is not conducive to timely drought response measures. In contrast, SPI/SPEI 12 can balance the calculation timescale and response time to appropriately reflect the region's drought conditions to a certain extent. SPI-12 can monitor droughts at seasonal and annual scales and better reflect the impact of seasonal precipitation changes on drought.

2.3. Temporal Analysis (Trend Analysis and Magnitude Change)

The Mann–Kendall (MK) statistical test, which is recommended by the World Meteorological Organization (WMO) for analyzing hydro-climatic data [47], is widely utilized as a non-parametric method for time series analysis. Unlike other tests, the MK test does not require the monitored data to adhere to specific distribution characteristics. The well-known non-parametric MK test [48,49] is frequently employed for identifying trends in hydro-meteorological time series data, such as rainfall, temperature, and drought indices [50]. This test is robust in detecting trends even when the temporal data do not follow a normal distribution and are unaffected by outliers. In this study, the MK analysis was employed to determine whether there was a statistically significant increasing or decreasing trend in SPI/SPEI-12 within a 95% confidence interval ($p < 0.05$) over a specific time period. Previous studies (e.g., Neeti et al. [51], Hamed et al. [52]) have noted that autocorrelations in time series can influence the results of the MK test. Interestingly, this study observed similar results despite accounting for autocorrelations. Additionally, the magnitude and extent of the trends in SPI and SPEI time series were assessed using the Theil–Sen slope estimator [53,54]. Finally, the results of the MK trend test for SPI and SPEI time series were incorporated into ArcMap v10.8 software (Esri, Redlands, CA, USA) to generate a spatial distribution of significant trends at individual locations. Furthermore, the Kriging method was employed to analyze decadal changes in SPI/SPEI-12. In our evaluation, we explored multiple models and semivariograms, ultimately determining that the exponential model combined with Kriging yielded the best results with low prediction errors for Sen's slope of SPI/SPEI.

The MK test determines whether there is a time series trend in the observed data by comparing the null hypothesis (H_0) and the alternative hypothesis (H_1). The statistical value S and the standardized test statistic Z_{MK} are computed in the MK test in the following way:

$$S = \sum_{i=1}^{n-1} \sum_{j=i+1}^n \text{sgn}(X_j - X_i) \quad (13)$$

$$\text{sgn}(X_j - X_i) = \begin{cases} +1 & \text{when } (X_j - X_i) > 0 \\ 0 & \text{when } (X_j - X_i) = 0 \\ -1 & \text{when } (X_j - X_i) < 0 \end{cases} \quad (14)$$

$$\text{Var}(S) = \frac{1}{18} \left[n(n-1)(2n+5) - \sum_{p=1}^q t_p(t_p-1)(2t_p+5) \right] \quad (15)$$

$$Z_{MK} = \begin{cases} \frac{S-1}{\sqrt{\text{Var}(S)}} & \text{when } S > 0 \\ 0 & \text{when } S = 0 \\ \frac{S+1}{\sqrt{\text{Var}(S)}} & \text{when } S < 0 \end{cases} \quad (16)$$

The MK test formulas utilize X_i and X_j to represent the corresponding values in the time series for years i and j . The length of the time series data is represented by n , while t_p represents the bundle value of the p th number. In the MK test, the trend of the time series data is determined by $Z_{MK} > 0$. If $Z_{MK} > 0$, it indicates an increasing trend in the time series data. Conversely, if $Z_{MK} < 0$, it represents a decreasing trend. When $|Z_{MK}| > Z_{(1-\frac{\alpha}{2})}$, the null hypothesis is rejected, and the time series data are deemed to have a significant trend. The value of $Z_{(1-\frac{\alpha}{2})}$ can be obtained from the standard normal distribution table. For instance, when $\alpha = 0.05$, the corresponding value of $Z_{(1-\frac{\alpha}{2})}$ is 1.96.

The Theil–Sen’s slope [54] estimator is a non-parametric method for estimating the slope of a linear regression model. It was introduced by Dutch economist Henri Theil [53] and American statistician Arthur Sen in the 1950s. This method is robust to outliers and does not require any assumptions about the distribution of the data. It can be particularly useful when the data contain outliers or when the relationship between the variables is not strictly linear.

The calculation of Sen’s method for linear slope is shown as follows:

$$\text{median}_{bi} = \frac{X_j - X_i}{j - i}, \text{ where } j > i \quad (17)$$

where X_j and X_i are the drought characteristic data values for years j and i ($j > i$), respectively. In Sen’s slope, the N values of b are ranked from smallest to largest, among which bi is the median of these N values, and Sen’s slope is defined as follows:

$$Q = \begin{cases} (b(N+1))/2 & N \text{ is odd} \\ (bN + N + 2)/4 & N \text{ is even} \end{cases} \quad (18)$$

2.4. Drought Identification and Characterization

The Run theory, proposed by Yevjevich et al. [55], is a widely used method for characterizing drought events [29]. A run is defined as a portion of a time series where all values remain below a selected threshold [35]. For this study, a drought event is defined according to McKee et al. [25] as consecutive negative SPEI/SPI values lasting at least one month, with the lowest SPEI/SPI less than -1 . Characterizing drought events is essential for several reasons. Firstly, prolonged droughts can have a significant impact on agriculture, vegetation growth, and the local environment [56]. Secondly, identifying drought events starting from negative SPEI/SPI values can be useful for enhancing drought early-warning systems.

The Run theory can be used to define and characterize a drought event based on its duration (DD), severity (DS), intensity (DI), and peak (DP). DD is calculated as the number of months between the start and end of the drought. DS is measured as the absolute sum of SPEI/SPI values during the drought period. DI is determined by calculating the average SPEI/SPI values within the drought duration, which is then divided by the duration. DP refers to the lowest SPEI value during the drought peak time (DPT). To analyze spatiotemporal drought characteristics, drought event indices are calculated based

on the Run theory at each station. The total number of drought events (DE) can then be determined, along with the mean drought duration (MDD), mean drought severity (MDS), mean drought intensity (MDI), and mean peak value (MDP) at individual stations. Regional drought mitigation can benefit from identifying the drought initiation season.

$$\text{MDD} = \frac{\sum_{i=1}^N DD_i}{N} \quad (19)$$

$$\text{MDS} = \frac{\sum_{j=1}^N DS_j}{N}, \text{ DS} = \sum_i^{DD} |SPEI_i| \text{ or } \text{DS} = \sum_i^{DD} |SPI_i| \quad (20)$$

$$\text{MDI} = \frac{\sum_{j=1}^N DI_j}{N}, \text{ DI} = \frac{\sum_i^{DD} |SPEI_i|}{DD} \text{ or } \text{DI} = \frac{\sum_i^{DD} |SPI_i|}{DD} \quad (21)$$

$$\text{MDP} = \frac{\sum_{j=1}^N DP_j}{N}, \text{ DP} = \max_{1 \leq i \leq DD} |SPEI_i| \text{ or } \text{DP} = \max_{1 \leq i \leq DD} |SPI_i| \quad (22)$$

The Formula (23) shows the calculation of drought severity and frequency using various parameters. Here, the drought duration for a single event is denoted as DD_i , while i represents a month within the drought event and $SPEI_i$ and SPI_i denote the SPEI and SPI values in that particular month, respectively. Additionally, DS , DI , and DP refer to drought severity, intensity, and peak value for a single drought event, respectively. During the study period, the number of observed drought events is represented by N , and j depicts one particular event. Furthermore, MDD, MDS, MDI, and MDP signify the mean duration, severity, intensity, and peak value of droughts during the specified time frame. By analyzing the percentage of drought locations in relation to the total number of study stations, we can identify areas that are more susceptible to droughts. This calculation also provides the percentage of stations affected by drought (SED) and is based on research conducted by Alsafadi et al. [57].

$$\text{SED}(\%) = \frac{m_i}{M_i} * 100 \quad (23)$$

The spatial extent of the drought, denoted by SED, is defined as the area where the number of drought stations (m_i) with $SPI/SPEI < 0$ or a specific intensity in month i is counted, out of the total number of stations (M_i) included.

2.5. Analysis of Spatial Autocorrelation Patterns (Moran's I Index)

To assess spatial autocorrelation patterns of drought characteristics in mainland China, the global Moran's I Index was utilized [58]. The standardized Z value was used to test the significance level of the global Moran's Index. The calculation formula [59] can be expressed as follows:

$$I = \frac{n}{\sum_{i=1}^n \sum_{j=1}^m w_{ij}} \frac{\sum_{i=1}^n \sum_{j=1}^m w_{ij} (x_i - \bar{x})^2}{(x_i - \bar{x})(x_j - \bar{x})} \quad (24)$$

$$Z_s = \frac{I - E(I)}{\sqrt{\text{VAR}(I)}} \quad (25)$$

where I represents the global Moran's Index, n is the total number of stations, \bar{x} is the average value of a drought characteristic for all stations, x_i and x_j represent the values of drought characteristics for the i -th and j -th stations, respectively, and w_{ij} is the weight coefficient assigned to stations i and j . $E(I)$ and $\text{VAR}(I)$ represent the expected value and variance of the Moran's Index. The global Moran's Index ranges between -1 and 1 . A positive value of the global Moran's Index greater than 0 ($p < 0.05$) indicates significant positive spatial autocorrelation among the drought characteristics of neighboring stations. On the

other hand, a negative value less than 0 ($p < 0.05$) indicates negative spatial autocorrelation. At a significance level of 0.05, if $|Z_S| > 1.96$, it indicates a significant global Moran's Index.

Anselin's local Moran's I Index [60] is used to perform clustering and analysis of discrete values, expressing the spatial aggregation characteristics of drought and the differences in regional drought autocorrelation [61].

To reflect the drought clustering types among different regions, the equation of local Moran's Index can be calculated as follows:

$$I_i = \frac{(x_i - \bar{x})}{\sum_i (x_i - \bar{x})^2} \sum_j w_{ij} (x_j - \bar{x}) \quad (26)$$

The significance level of the local Moran's Index can be tested by calculating the Z value using the above formula. If the local spatial autocorrelation is significant, it indicates that there is a certain clustering relationship between the drought characteristic value in a station and that in the surrounding stations. The clustering relationships can be classified into four types: high-high clustering (H-H), low-low clustering (L-L), high-low outliers (H-L), and low-high outliers (L-H).

3. Results and Analysis

3.1. Temporal and Spatial Variability of Droughts

The Mann–Kendall (MK) test was used in this study to track the temporal trend of the SPI and SPEI, and the SPI trend results indicated that 477 of the 700 stations had significant positive/negative values, accounting for 68.14% of all stations: 41.3% of total stations had significant negative trends, while 23.4% of total stations had significant positive trends. On the other hand, there were 552 significant stations in the SPEI data, accounting for 78.86% of all stations: 64.3% of total stations had significant negative trends, while only 14.57% of total stations had significant positive trends.

According to Figure 2a, based on the trend results of SPI-12 per decade, most of the sites near the Hu Huanyong Line [62] show a downward trend, while the northwest, Qinghai–Tibet Plateau, and southeastern regions of China show an upward trend. Most areas in Beijing, Tianjin, Liaoning Province, Henan Province, and Shandong Province show a downward trend. The highest positive Sen's slope values are distributed in the northeastern Qinghai–Tibet Plateau and eastern Xinjiang, while the lowest Sen's slope values are distributed around Liaoning Province, Beijing City, and Tianjin City. Overall, the trend of SPI-12 in mainland China is mostly upward, with a few areas showing a downward trend, and the magnitude of the upward trend is high, while the magnitude of the downward trend is low.

Interestingly, according to the trend of SPEI12 per decade, there are more sites showing a downward trend in mainland China compared to SPI-12 trend results (Figure 2b), except for some areas in the Qinghai–Tibet Plateau, northern Xinjiang, and southeastern China showing an upward trend. While, the vast majority of sites north of the Qinling–Huaihe Line [63] show a downward trend, and areas such as Yunnan Province, Sichuan Province, and Chongqing Municipality show a downward trend. In the areas where the upward trend is apparent, the most evident upward trend is in the northeastern Qinghai–Tibet Plateau, similar to the results of SPI-12. However, in the areas where the downward trend is evident, the most significant downward trend is in southern Xinjiang, western Inner Mongolia, Beijing, Tianjin, southern Liaoning Province, and eastern Shandong Province. Among them, the trend of SPI-12 and SPEI-12 is opposite in southern Xinjiang and western Inner Mongolia, while the trend is the same in Beijing, Tianjin, southern Liaoning Province, and eastern Shandong Province.

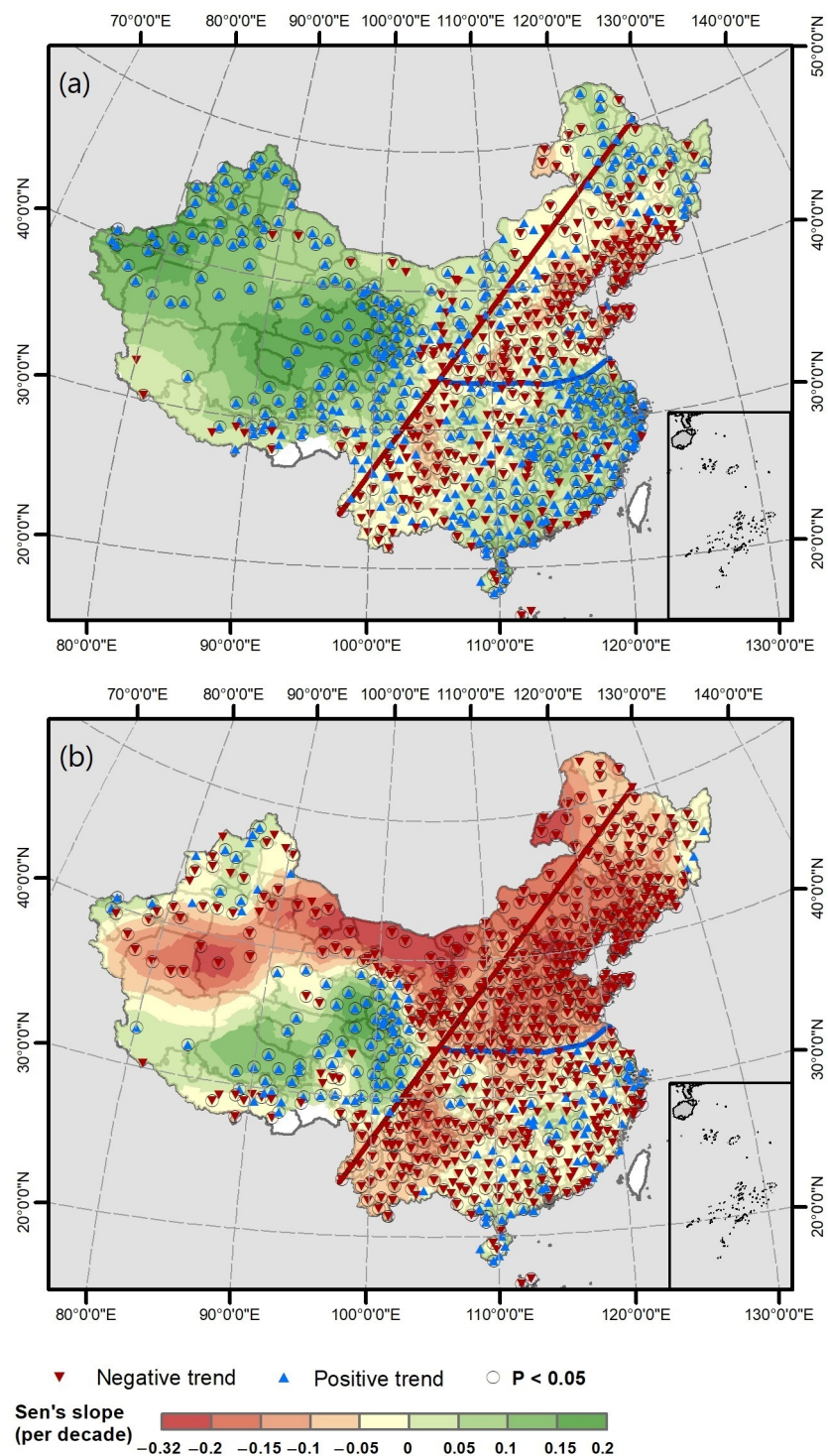


Figure 2. The decadal change and trend of SPI-12 (a) and SPEI-12 (b) in China mainland between 1951 and 2020. The red line indicates the Hu Huanyong Line, and blue line indicates the Qinling–Huaihe Line.

3.2. Percentage of Stations Affected by Drought

The SPI-based spatial extent of drought or percentage of stations affected by drought illustrates the vulnerability of different drought classes over mainland China. According to Figure 3, the percentage of stations impacted by all drought classes decreased during the study period, and this decrease was statistically significant ($p < 0.05$) for mild drought, moderate drought, and severe drought. However, the percentage of stations influenced by

wet conditions (i.e., $SPI > 0$) showed an upward trend from 1951 to 2020, with an increase of 1% per decade ($p < 0.05$). A comparison between the different drought classes suggests that the decreases in the percentage of stations impacted by mild drought, moderate drought, and severe drought were stronger than those of extreme and very extreme droughts. For example, the percentage of stations influenced by mild drought decreased by -0.47% per decade, while severe drought and moderate drought decreased by 0.28% and 0.14% , respectively.

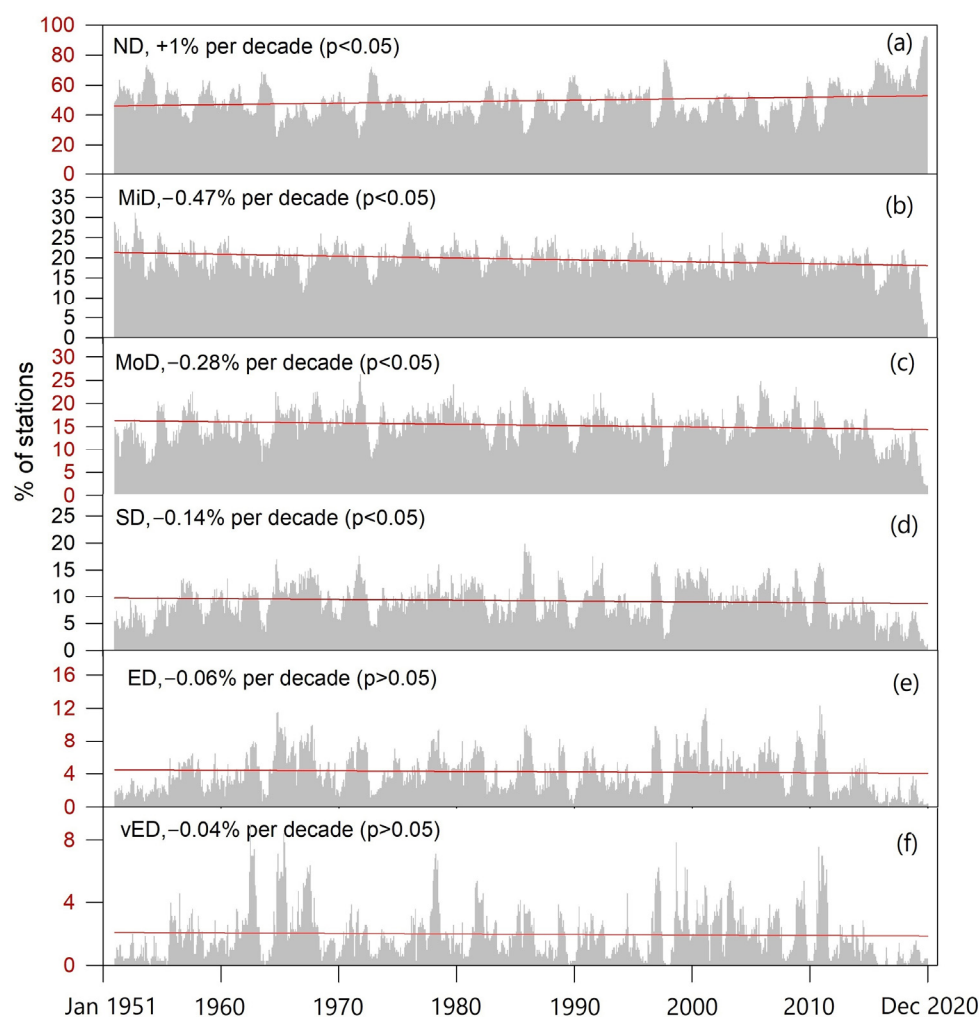


Figure 3. Temporal evolution of the spatial extent of area (% of stations) impacted by multiple drought categories based on the SPI-12 timescale over mainland China between 1951 and 2020. (Sub-figures from (a–f) are based on Table 1).

Table 1. Drought categories based on McKee’s scheme [25].

SPI and SPEI Values	Drought Category
>0	No drought (ND)
0 to -0.5	Mild drought (MiD)
-0.5 to -1	Moderate drought (MoD)
-1 to -1.5	Severe drought (SD)
-1.5 to -2	Extreme drought (ED)
>-2	Very extreme drought (vED)

Figure 4 illustrates the vulnerability of different drought classes in mainland China between 1951 and 2020. Interestingly, the results are opposite to those reflected by the SPI. During the study period, except for mild drought, the percentage of stations impacted by

all other drought classes exhibited an increasing trend, and this increase was statistically significant ($p < 0.05$). The percentage of stations affected by mild drought exhibited a decreasing trend, with a decrease of -0.17% per decade ($p < 0.05$). However, the percentage of stations influenced by wet conditions (i.e., $\text{SPEI} > 0$) showed a downward trend from 1951 to 2020, with a decrease of -2.8% per decade ($p < 0.05$). A comparison between the different drought classes suggests that the increases in the percentage of stations impacted by moderate, severe, and extreme droughts were stronger than those of very extreme droughts. For example, the percentage of stations influenced by moderate drought increased by 0.6% per decade, compared to 1.12% and 0.94% for severe and extreme droughts, respectively. Notably, during the extraordinary drought period from 2010 to 2011, the percentage of stations impacted by severe drought ($-1 < \text{SPEI} < -1.5$) and extreme drought ($-1.5 < \text{SPEI} < -2$) was both around 20% , and the percentage of stations affected by very extreme drought ($\text{SPEI} > -2$) was around 10% .

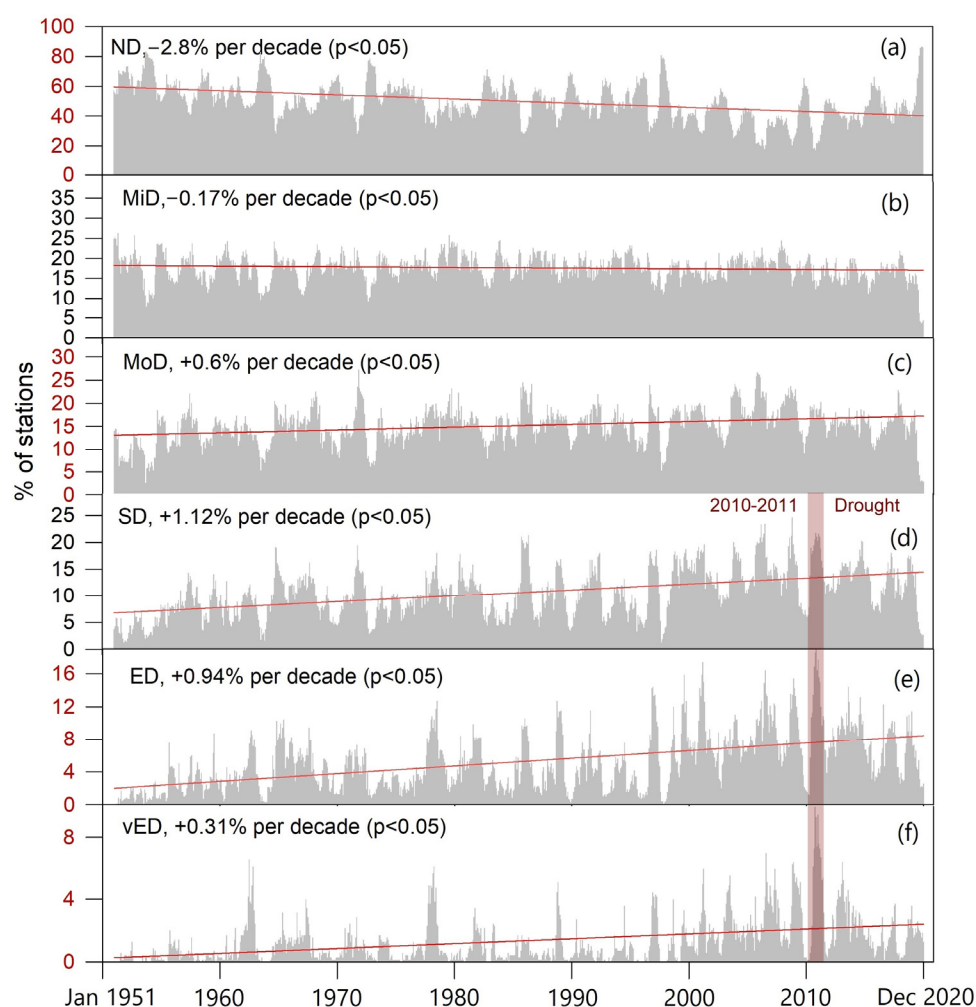


Figure 4. Temporal evolution of the spatial extent of area (% of stations) impacted by multiple drought categories based on the SPEI-12 timescale over mainland China between 1951 and 2020. (Sub-figures from (a–f) are based on Table 1).

3.3. SPEI-12-Based Spatial Extent of 2010–2011 Extreme Drought

According to Figure 5, a severe drought event occurred in China from September 2010 to December 2011. The panel in the upper left shows that in August 2011 (Figure 5a), based on SPEI12 data, severe drought in mainland China was mainly concentrated in southern China, such as Shaanxi, Shanxi, Henan, and Anhui provinces. The drought did not weaken in September and October 2011, and the number of extremely dry stations increased. By

November and December 2011, the drought had retreated to southern China south of the Qinling–Huaihe Line, and the overall drought level in China began to decrease. The bar chart in the lower right corner shows the percentage of multi-class affected by drought. The percentage of stations with no drought decreased from 18% at the beginning to 17% in October and then increased to 22% in December. Almost 80% of China’s meteorological stations were in a state of drought. The proportion of extreme drought increased from 17% in August to 21% in October and then decreased to 17% in December. The proportion of extremely severe drought increased from 7% in August to 11% in September and then decreased to 7% in November and increased to 9% in December.

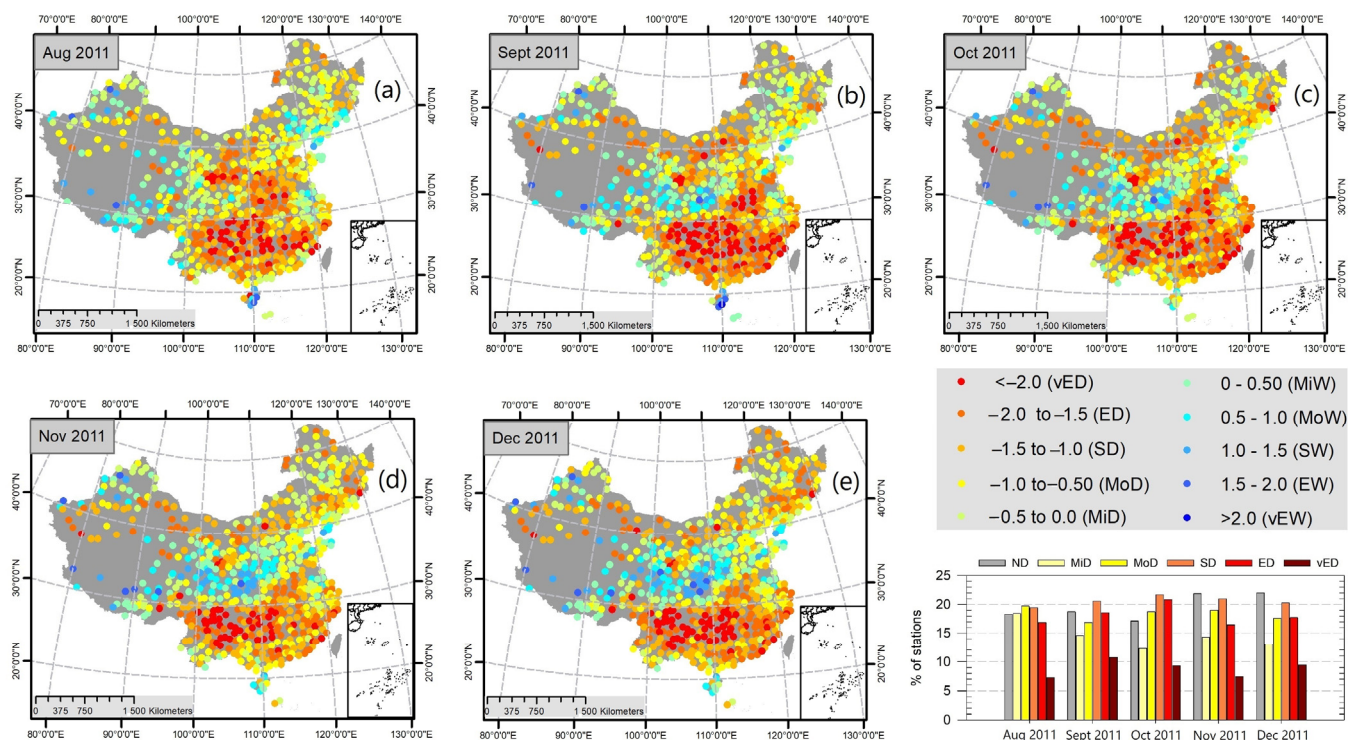


Figure 5. Spatial-temporal variability of SPEI-12 and spatial extent of the extreme drought event that occurred in mainland China from 2010 to 2011. Note: Subpanels from (a–e) indicate the temporal evolution of the 2010 to 2011 extreme drought event.

3.4. SPI-12 and SPEI-12-Based Spatial Patterns of Drought Characteristics

To analyze the SPI-12-based spatial autocorrelation of the total number of drought events (TDE) between 1951 and 2020, the global Moran’s I Index was used. The z-score was 22.366, so there is a less than 1% likelihood that this clustered pattern could be the result of random chance. Based on the local spatial autocorrelation of the TDE and using Anselin’s local Moran’s I Index, the results indicated the presence of four spatial patterns. The northwest, Qinghai–Tibet Plateau, and northeast China have fewer events with two main clustering patterns (Low-Low cluster and High-Low outlier), which means that these regions have a lower frequency of drought events, while the southern region has more total drought events with two main clustering patterns (High-High cluster and Low-High outlier), which means that these regions have a higher frequency of drought during the studied period (see Figure 6a,c).

As shown in Table 2, the z-score of spatial autocorrelation of MDD based on SPI-12 analysis is 17.648, indicating that the probability of this clustering pattern being the result of random factors is less than 1%. From Figure 7a, it can be observed that the duration of drought in northern China is longer than that in the southern region. On the other hand, as shown in Figure 7a,e, four spatial patterns were identified based on the local spatial autocorrelation of MDD. In northwestern Xinjiang, southeastern Qinghai–Tibet plateau, and northeastern China, the duration of drought is longer, exhibiting two cluster patterns (High-High cluster and Low-High outlier), indicating that the duration of drought is longer in northern China. In southern China, except for the middle and lower reaches of the Yangtze River, the duration of drought is shorter, exhibiting two cluster patterns (Low-Low cluster and High-Low outlier).

According to Table 2, the SPI-12-analysis-based MDP exhibits a spatial autocorrelation z-score of 2.051, suggesting that the likelihood of this clustering pattern resulting from random factors is 4%. No significant clustering features can be observed in Figure 7b. On the other hand, based on the local spatial autocorrelation of the MDP as shown in Figure 7b,f, meaningful results were only observed in northern China, where four spatial patterns appeared. In Xinjiang, central Inner Mongolia, and southern northeast China, two clustering patterns (High-High cluster and Low-High outlier) were observed, indicating relatively small MDP and drought impacts in these regions. In Qinghai and Shanxi provinces, two clustering patterns (Low-Low cluster and High-Low outlier) were observed, indicating an increase in MDP and drought impacts in these provinces over the past 70 years.

Table 2 displays that the SPI-12-analysis-based MDS has a z-score of 18.12 for spatial autocorrelation, which implies that the probability of this clustering pattern resulting from random factors is below 1%. A west-high and east-low trend can be observed along the Hu Huanyong Line in Figure 7c. On the other hand, four spatial patterns of local spatial autocorrelation based on MDS are observed in Figure 7c,g. Two clustering patterns (High-High cluster and Low-High outlier) are observed in the northwest of Xinjiang, southeast of the Qinghai–Tibet Plateau, and northeast of China, indicating that these regions have a higher severity of drought. Two clustering patterns (Low-Low cluster and High-Low outlier) are observed in the area south of the Qinling–Huaihe Line and east of the Hu Huanyong Line, but no clustering pattern is found in the middle and lower reaches of the Yangtze River, indicating that the severity of drought in these regions is relatively low.

Table 2 displays a z-score of 10.267 for the spatial autocorrelation of MDI as determined by the SPI-12 analysis. This suggests that the likelihood of this clustered pattern being caused by chance factors is below 1%. From Figure 7d, it is difficult to observe the clustering trend of drought intensity. On the other hand, as shown in 7d,h, based on MDI's local spatial autocorrelation, only four spatial patterns were observed in northern China, indicating meaningful results. In the middle and lower reaches of the Yangtze River, two clustering patterns were found (High-High cluster and Low-High outlier), indicating that the drought intensity in this region is relatively low, which is the lowest in China. In the southern part of the Qinghai–Tibet Plateau, Shaanxi Province, Shanxi Province, Henan Province, Shandong Province, and the southern part of Heilongjiang Province, two clustering patterns were found (Low-Low cluster and High-Low outlier), indicating that the severity of drought in these regions is relatively high.

Based on Table 2, the SPEI12 analysis indicates that the spatial autocorrelation z-score for MDD is 18.233. This suggests that it is highly unlikely for this clustering pattern to be the result of chance factors, with a probability of less than 1%. From Figure 8a, it can be observed that the duration of drought in northern China is longer than that in the south. On the other hand, as shown in Figure 8a,e, four spatial patterns were identified based on the local spatial autocorrelation of MDD. In Xinjiang, Qinghai, Beijing, Tianjin, Hebei, Liaoning, and eastern Shandong, two clustering patterns (High-High cluster and Low-High outlier) were identified, indicating that drought duration in these areas is longer. In southern China, two clustering patterns (Low-Low cluster and High-Low outlier) were identified, indicating that drought duration in these areas is shorter.

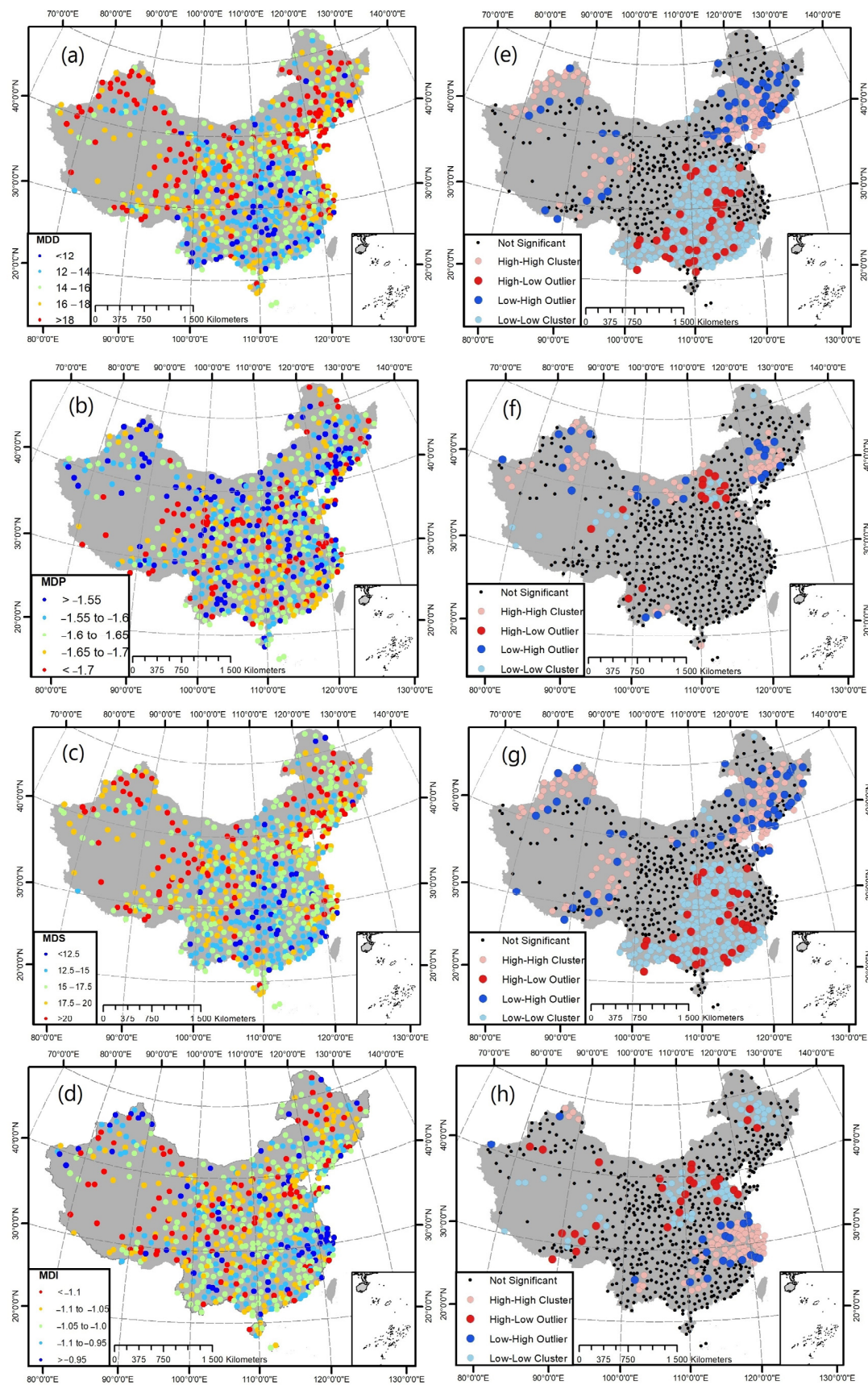


Figure 7. Spatial distribution of MDD, MDP, MDS, and MDI ((a–d), respectively) and the clustering patterns ((e–h), respectively) in mainland China over the past 70 years based on SPI-12 between 1951 and 2020.

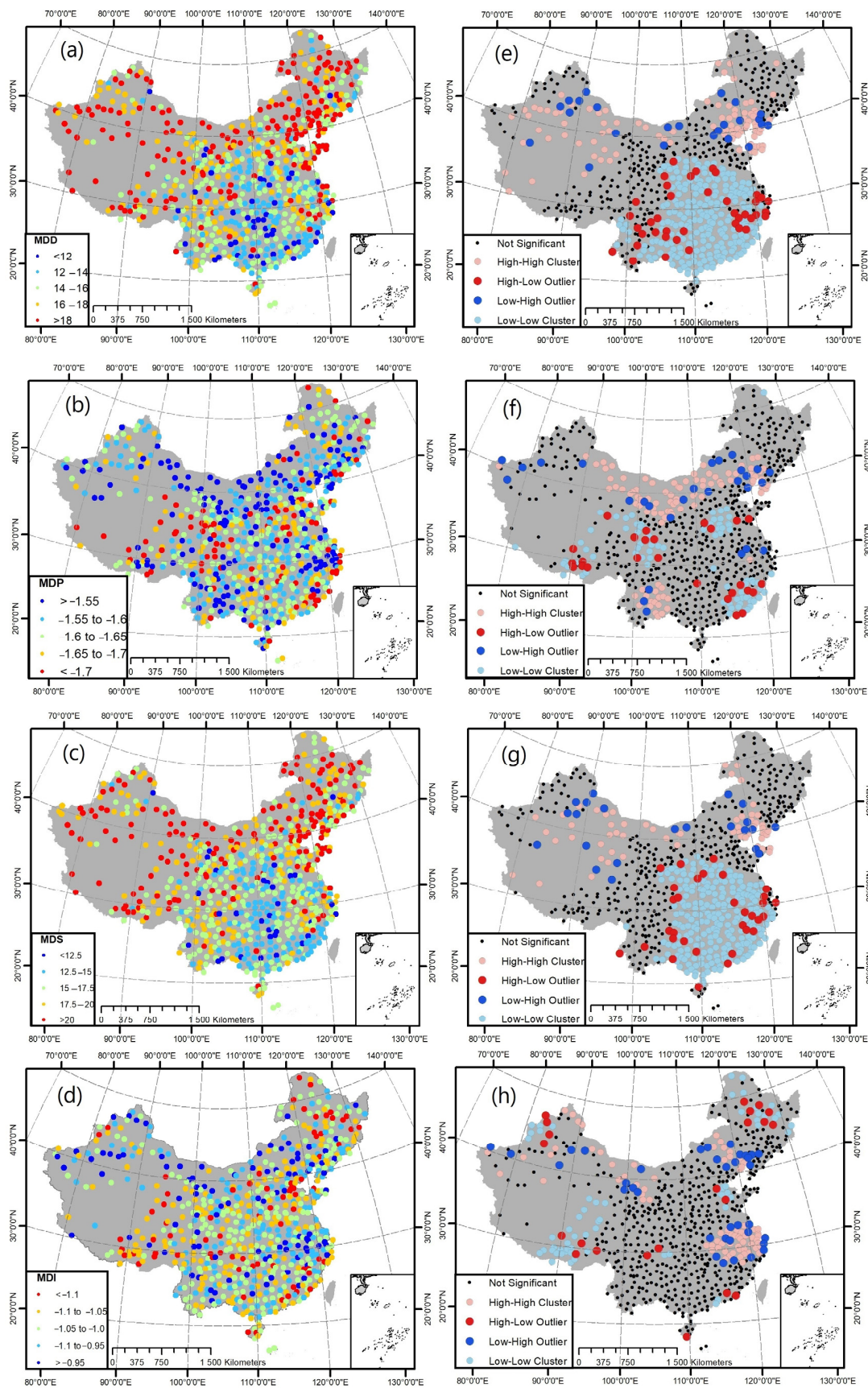


Figure 8. Spatial distribution of MDD, MDP, MDS, and MDI ((a–d), respectively) and the clustering patterns ((e–h), respectively) in mainland China over the past 70 years based on SPEI-12 between 1951 and 2020.

According to the SPEI-12 analysis, the spatial autocorrelation of MDP is represented in Table 2 by a z-score of 11.054. This value suggests that the likelihood of the observed clustering pattern happening randomly is extremely low, with a probability of less than 1%. No significant clustering features were observed in Figure 8b. On the other hand, as shown in Figure 8b,f, four spatial patterns of MDP's local spatial autocorrelation emerged. In Inner Mongolia, Liaoning Province, and Yunnan Province, two clustering patterns (High-High cluster and Low-High outlier) were observed, implying that MDP values were low and extreme drought values were minimal in the past 70 years. In southern Tibet, Sichuan Province, Henan Province, and Fujian Province, two clustering patterns (Low-Low cluster and High-Low outlier) were observed, indicating that MDP values were low during the most extreme drought periods in the past 70 years.

As per the SPEI12 analysis, Table 2 presents a spatial autocorrelation z-score of 14.629 for MDS, implying that the observed clustering pattern is highly unlikely to have arisen by chance, with a probability of less than 1%. From Figure 8c, it was found that the severity of drought in northern China is greater than that in southern China. On the other hand, as shown in Figure 8c,g, four spatial patterns were observed based on the local spatial autocorrelation of MDS. Two clustering patterns (High-High cluster and Low-High outlier) were found in the northwest region, Jing-Jin region, southern Liaoning, and eastern Shandong, indicating that drought is more severe in these areas. Two clustering patterns (Low-Low cluster and High-Low outlier) were found in southern China, indicating that the severity of drought in the region is relatively low.

As presented in Table 2, the z-score for spatial autocorrelation of MDI, using the SPEI12 analysis, is 7.421, signifying that the likelihood of this clustering pattern being a result of random factors is less than 1%. From Figure 8d, it can be seen that drought is more severe in northern China than in the south. On the other hand, based on the local spatial autocorrelation of MDI, only meaningful results were observed in northern China, where four spatial patterns appeared, as shown in Figure 8d,h. Two clustering patterns (High-High cluster and Low-High outlier) were observed in southern Xinjiang, northern Gansu, the middle and lower reaches of the Yangtze River, Liaoning Province, and northern Inner Mongolia, indicating relatively lower drought intensity in these areas over the past 70 years. Two clustering patterns (Low-Low cluster and High-Low outlier) were observed in some areas of northwest Xinjiang, southeastern Qinghai–Tibet Plateau, Heilongjiang Province, western Shandong Province, and Chongqing City, indicating higher drought intensity in these areas.

Overall, the characteristics of drought in China are that the frequency of drought in the northern region is low and its duration is long, while the frequency of drought in the southern region is high and its duration is short. Additionally, various drought indicators analyzed based on SPEI12 are more concerning than those analyzed based on SPI-12.

4. Discussion

4.1. Inconsistency in Distinguished Trend Patterns of SPI/SPEI over China

It is significant to analyze the impacts of drought and identify and characterize factors such as intensity, severity, spatial extent, and duration at regional and national scales [64]. The benefits and drawbacks of using a particular drought index might vary greatly. Drought due to a lack of precipitation can be more accurately reflected by the SPI. In some investigations of drought in China, Tan et al. [65] and Li et al. [33] found that the SPEI was more applicable than the SPI. To evaluate recent historical trends for these drought indices, this article used Mann–Kendall statistical test and Sen's slope method based on SPI-12 and SPEI-12. Our findings revealed significant differences in the change trends of drought-prone areas based on SPI and SPEI in mainland China, specifically when considering the SPEI-based water balance. These differences can be attributed to the inclusion of additional climatic factors, such as temperature and evapotranspiration, in the calculation of SPEI. As a result, the distribution of drought events and their temporal trends in China, as indicated

by SPEI, raise greater concerns related to the effects of global warming. These results align with the findings reported by Alsafadi et al. [51] and Mohammed et al. [66] in other regions.

In China, some studies have reported the same findings. It is worth noting that there are many differences in the results of SPI-12 and SPEI-12, such as spatiotemporal variability of drought. For example, Feng et al. [67] documented that both SPI-12 and SPEI-12 show a trend towards increasing in some regions of the Qinghai–Tibet Plateau and the southeastern coast of China. Although the Qinghai–Tibet Plateau is high in altitude, low in temperature, and low in precipitation, evaporation is also low, which explains why SPI and SPEI show similar trends based on this region. In some sparsely populated areas of the southeastern coast, the SPI shows positive trends higher than that presented in SPEI positive trends. This may be due to increasing precipitation extremes indices as explained by Wang et al. [68]. The risk of extreme events may increase. Interestingly, the results based on SPI-12 also show a positive trend in some areas, such as southern Xinjiang, Inner Mongolia, and Heilongjiang. This aligns with the findings reported by Li et al. [69] in Northwest China from 1960 to 2018, while SPEI-12 shows a negative trend. This may be due to drought caused by increasing population densities and industry development in southern Xinjiang, which may have indirect effects on the evolution of drought [70].

As such, one of the reasons for drought intensification is the effect of urbanization on extreme precipitation and drought events. The Hu Huanyong Line, as an important boundary line for the distribution of China's population, coincides very well with the boundary line between trends towards drying and trends towards wetting in this study, indicating that drought may be closely related to the impact of urbanization and human activities on temperature and evapotranspiration. The urban heat island effect may affect urban precipitation patterns. For example, in the Yangtze River urban belt in China, the downstream propagation of urban heat island signal alters the general circulation pattern, thermal distribution, and moisture transportation at local and regional scales [71,72]. The urbanization pattern of cities has a key effect on precipitation intensity and gives rise to extreme precipitation. On the other hand, high temperatures increase evaporation rates, while cooling requires more evaporation, further exacerbating drought conditions [73,74]. There is a significant spatiotemporal variability in the distribution of drought in China. The most severe drought occurs in the northwest, followed by the western part of the southwestern region and the northern part of the North China Plain [42]. On the other hand, urban development often uses impermeable materials (such as asphalt and concrete) instead of natural vegetation and permeable soil surfaces, which weaken the heat exchange between the air and the ground surface, trap urban heat, and increase evaporation [75,76]. This study shows that the area affected by drought based on SPI-12 gradually exhibits insignificant decreases per decade, while SPEI-12 shows the opposite trend, which also reflects the impact of urbanization caused by China's economic development on the changes in drought. In densely populated urban areas, urban drought is caused by the increase in water demand from a large population and various urban departments [77], which is consistent with the conclusion of this study, namely, the drought line coincides with the population density line.

4.2. Extreme Drought and Spatial Patterns of Drought Characteristics

During the period from 1961 to 2000, the extreme drought event in September 1965 was the most severe, affecting nearly half of China's land area [78]. In this study, and based on the 1951–2020 period, we found that the most severe drought in China occurred in 2010–2011 affecting nearly 80% of China mainland. The frequency of drought in China gradually decreases from south to north, with fewer occurrences in the northeast and northern regions. However, the duration and severity of drought in these regions are longer and more severe [79]. Mokhtar et al. [40] calculated the drought in Tibetan Plateau, China from 1980 to 2019 using SPEI and found that extreme and extremely high severity droughts have affected more than 30% of the area studied. In addition, the drought's geographical distribution spanned 80–90% of the region under study between 2015 and 2019.

For more insights, this study explained the spatial patterns of drought characteristics in China (Figures 7 and 8) between 1951 and 2020 using the global Moran's Index and local Moran's Index. The study found that in the northwest and northeast regions of China, droughts are long-lasting, with high severity, with low frequency, low peak, and low intensity, while in the southern regions of China, droughts are short-lasting, with low severity, with high frequency, high peak, and high intensity. In general, drought may be caused by ocean and atmospheric circulation patterns. ENSO refers to the natural phenomenon of abnormal warming of sea surface temperature in the central and eastern Pacific [80]. This phenomenon usually occurs every 2–7 years and has important impacts on the global climate system [81]. The occurrence of El Niño and La Niña may be closely related to the increase in spring and summer drought frequency in northern China [82]. During the development stage of ENSO, precipitation in northern China is generally low, which may lead to drought. The precipitation in northern China usually concentrates in summer, and when ENSO affects the summer in northern China, it will reduce summer precipitation in northern China, causing the duration of drought to become longer, corresponding to the long duration of drought in northern China in this study. The increase in autumn drought frequency in southern China is mainly due to the influence of ENSO [83]. ENSO events affect summer droughts in the middle and upper reaches of the Pearl River and autumn droughts in the Pearl River Delta [84], which may affect the peak and frequency of droughts in southern China, making the peak of droughts in southern China high with frequent occurrence.

In the past 40 years, China's total grain output has increased by 74%, exceeding the population growth by about 34% [85], but the increase in severe drought occurrence in China will double the loss rate of crop yield caused by drought [86,87]. Meanwhile, drought can lead to water shortages and food crises, affecting social stability and exacerbating economic difficulties and unfairness in rural areas [88,89]. For example, drought in high-latitude regions is also worth attention; for example, in Heilongjiang Province—as a major agricultural province in China—the risk of agricultural drought will continue to exhibit a decreasing trend [88]. Inner Mongolia Autonomous Region, as a major province in livestock production and forest areas in China, is located on the edge of the East Asian monsoon climate and the continental climate. The detected drought tendency may bring critical negative impacts on ecological systems and carbon storage [90]. Therefore, the government should control the unnecessary expansion of the livestock industry and ensure its sustainable development.

5. Conclusions

The present study systematically investigated drought characteristics with emphasis on its propagation patterns and historical trends over China during the last 70 years. To achieve this, the study employed observed station data derived from 752 synoptic stations distributed across the study domain. As the first step, the datasets were processed with missing data corrected using gridded observations obtained from the GPCP database. Eventually, 700 stations with valid datasets were used to compute the SPI and SPEI at 12 timescales (i.e., SPEI-12 and SPI-12). Trends analysis was estimated using the non-parametric approach of MK analysis, whereas the magnitude of the trends was detected using the Theil–Sen Slope estimator. Furthermore, the study employed the Run theory framework to characterize drought patterns in terms of mean drought duration, severity, intensity, and peak during the study duration over China. Ultimately, we used global Moran's I Index and Anselin's local Moran I Index to construct the drought propagation patterns and reflect the drought clustering types over different regions across the study area. Our findings reveal a noteworthy increase in the magnitude of drought trends, with 68.14% (78.86%) of total station data depicting upward/downward SPI (SPEI) values. The drought trends result over China is more concerning based on the SPEI, where 64.3% of total stations had significant negative trends, while only 14.57% of total stations had significant positive trends, which indicates the warming effects in the last decades. Particularly,

droughts in northern China have lower frequency but longer durations, while droughts in southern China have higher frequency but shorter durations. Interestingly, northeastern Qinghai–Tibet Plateau depicts upward tendencies based on SPI and SPEI, while opposite trends (negative trends) are observed in regions of Yunnan Province, Sichuan Province, and Chongqing Municipality in addition to Shandong and Hebei, Shanxi, and Henan provinces and Beijing and Tianjin cities. Meanwhile, the spatial extent of drought based on SPI/SPEI-12 shows a contrasting pattern with SPI-12, indicating a decline in the percentage of stations impacted by different drought categories, except extreme and very extreme droughts, while SPEI-12 depicts an increase in the percentage of stations impacted by all other drought classes, except for mild drought. Finally, during the clustering analysis, we established that drought events occur less frequently in eastern Xinjiang, western Gansu, and western Inner Mongolia. This may be due to the fact that these regions are relatively drier compared to other areas in China, and as such, the conditions required for drought to occur are higher, resulting in a lower frequency of drought events. On the other hand, southern China experiences more drought events. It is important to note that drought is relative and not absolute.

The study findings suggest several recommendations aimed at assisting decision-makers in effectively managing drought events. These recommendations can be summarized as follows:

- (i) **Management of Water Resources:** Enhance the management and protection of water resources. This can be achieved by implementing measures to modernize irrigation systems, thereby improving water efficiency and reducing water loss.
- (ii) **Water Conservation Measures:** Implement water conservation measures across various sectors, including residential, agricultural, and industrial areas. Examples of such measures include promoting the use of water-saving toilets, advocating for garbage classification, and encouraging the installation of household water storage tanks in dry regions with extended drought periods, particularly in northern China.
- (iii) **Scientific Farming:** Focus on the development of drought-resistant crops and the adoption of more scientific farming techniques. This includes improving crop drought resistance and yield through the implementation of flexible agricultural management measures.
- (iv) **Appropriate Planting Methods:** During drought periods, it is crucial to choose appropriate planting methods, such as using insulation to cover crops or employing drip irrigation technology. These methods can help conserve moisture and reduce water usage.
- (v) **Strengthen Monitoring and Early Warning Systems:** Enhance monitoring and early warning systems for drought. This involves promptly identifying drought situations, predicting the severity and extent of drought, and implementing suitable protective measures based on the information gathered.
- (vi) **Resource Sharing:** Strengthen international cooperation and establish multilateral and bilateral resource-sharing mechanisms to collectively address the challenges posed by drought.

In addition, future research directions could involve studying the relationship between drought and its influence on socioeconomic, cultural, and agricultural development in specific provinces. This would enable a better understanding of the impact of drought on human society and facilitate more effective countermeasures. By implementing these recommendations and undertaking further research, decision-makers can enhance their ability to manage and mitigate the impacts of drought events, contributing to the resilience and sustainability of communities and regions affected by drought.

Author Contributions: Conceptualization, K.A.; methodology, K.A.; software, K.A. and J.S.; formal analysis, K.A. and J.S.; investigation, K.A.; data curation, J.S., S.B., Z.G., K.W. and K.A.; writing—original draft preparation, K.A., B.O.A. and J.S.; writing—review and editing, K.A., S.B., B.B. and A.A.; visualization, K.A.; supervision, S.B.; funding acquisition, A.A., B.B. and S.B. All authors have read and agreed to the published version of the manuscript.

Funding: This work was supported by the National Natural Science Foundation of China (grant numbers 41971340 and 41271410) and also by the Researchers Supporting Project (grant number RSP2023R296), King Saud University, Riyadh, Saudi Arabia.

Data Availability Statement: The data that support the findings of this study are available upon request.

Conflicts of Interest: The authors declare no conflict of interest.

Appendix A

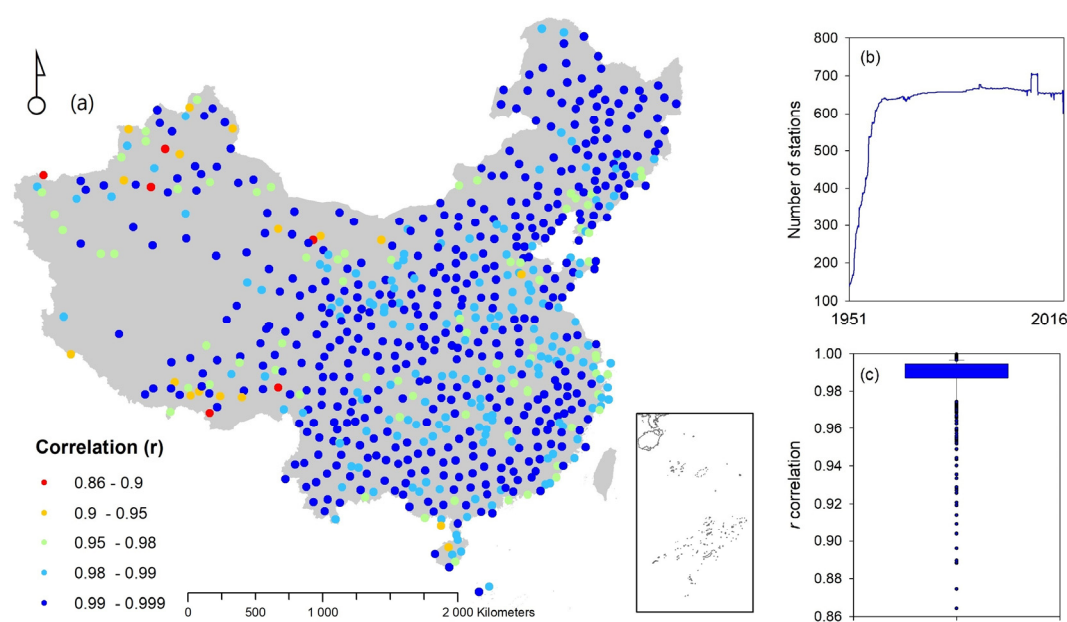


Figure A1. (a) Spatial–temporal correlation between observed precipitation data and GPCP data during 1951–2016 period. (b) Number of stations for each month within the observed precipitation time series data (This panel indicates the structure of missing values that has been corrected.). (c) Boxplot of correlation between observed precipitation data and GPCP data.

References

- Schewe, J.; Heinke, J.; Gerten, D.; Haddeland, I.; Arnell, N.W.; Clark, D.B.; Dankers, R.; Eisner, S.; Fekete, B.M.; Colón-González, F.J.; et al. Multimodel Assessment of Water Scarcity under Climate Change. *Proc. Natl. Acad. Sci. USA* **2014**, *111*, 3245–3250. [[CrossRef](#)] [[PubMed](#)]
- Pedro-Monzonís, M.; Solera, A.; Ferrer, J.; Estrela, T.; Paredes-Arquiola, J. A Review of Water Scarcity and Drought Indexes in Water Resources Planning and Management. *J. Hydrol.* **2015**, *527*, 482–493. [[CrossRef](#)]
- Shi, H.; Chen, J.; Wang, K.; Niu, J. A New Method and a New Index for Identifying Socioeconomic Drought Events under Climate Change: A Case Study of the East River Basin in China. *Sci. Total Environ.* **2018**, *616–617*, 363–375. [[CrossRef](#)] [[PubMed](#)]
- Luo, L.; Apps, D.; Arcand, S.; Xu, H.; Pan, M.; Hoerling, M. Contribution of Temperature and Precipitation Anomalies to the California Drought during 2012–2015. *Geophys. Res. Lett.* **2017**, *44*, 3184–3192. [[CrossRef](#)]
- Mokhtar, A.; He, H.; Alsafadi, K.; Li, Y.; Zhao, H.; Keo, S.; Bai, C.; Abuarab, M.; Zhang, C.; Elbagoury, K.; et al. Evapotranspiration as a Response to Climate Variability and Ecosystem Changes in Southwest, China. *Environ. Earth Sci.* **2020**, *79*, 312. [[CrossRef](#)]
- Dai, A.; Zhao, T.; Chen, J. Climate Change and Drought: A Precipitation and Evaporation Perspective. *Curr. Clim. Chang. Rep.* **2018**, *4*, 301–312. [[CrossRef](#)]
- Qiang, Z.; Lanying, H.; Jingjing, L.; Qingyan, C. North–South Differences in Chinese Agricultural Losses Due to Climate-Change-Influenced Droughts. *Theor. Appl. Clim.* **2018**, *131*, 719–732. [[CrossRef](#)]
- Zhang, T.; Huang, Y. Impacts of Climate Change and Inter-Annual Variability on Cereal Crops in China from 1980 to 2008. *J. Sci. Food Agric.* **2012**, *92*, 1643–1652. [[CrossRef](#)]

9. Ye, T.; Shi, P.; Wang, J.; Liu, L.; Fan, Y.; Hu, J. China's Drought Disaster Risk Management: Perspective of Severe Droughts in 2009–2010. *Int. J. Disaster Risk Sci.* **2012**, *3*, 84–97. [[CrossRef](#)]
10. Lu, E.; Luo, Y.; Zhang, R.; Wu, Q.; Liu, L. Regional Atmospheric Anomalies Responsible for the 2009–2010 Severe Drought in China: The 2009–2010 Severe Drought in China. *J. Geophys. Res. Atmos.* **2011**, *116*, D21114. [[CrossRef](#)]
11. Lü, J.; Ju, J.; Ren, J.; Gan, W. The Influence of the Madden-Julian Oscillation Activity Anomalies on Yunnan's Extreme Drought of 2009–2010. *Sci. China Earth Sci.* **2012**, *55*, 98–112. [[CrossRef](#)]
12. Yang, J.; Gong, D.; Wang, W.; Hu, M.; Mao, R. Extreme Drought Event of 2009/2010 over Southwestern China. *Meteorol. Atmos. Phys.* **2012**, *115*, 173–184. [[CrossRef](#)]
13. Leng, G.; Tang, Q.; Rayburg, S. Climate Change Impacts on Meteorological, Agricultural and Hydrological Droughts in China. *Glob. Planet. Chang.* **2015**, *126*, 23–34. [[CrossRef](#)]
14. Song, Z.; Xia, J.; She, D.; Li, L.; Hu, C.; Hong, S. Assessment of Meteorological Drought Change in the 21st Century Based on CMIP6 Multi-Model Ensemble Projections over Mainland China. *J. Hydrol.* **2021**, *601*, 126643. [[CrossRef](#)]
15. Gong, X.; Du, S.; Li, F.; Ding, Y. Study on the Spatial and Temporal Characteristics of Mesoscale Drought in China under Future Climate Change Scenarios. *Water* **2021**, *13*, 2761. [[CrossRef](#)]
16. Zhang, Y.; Hu, X.; Zhang, Z.; Kong, R.; Peng, Z.; Zhang, Q.; Chen, X. The Increasing Risk of Future Simultaneous Droughts over the Yangtze River Basin Based on CMIP6 Models. *Stoch. Environ. Res. Risk Assess.* **2023**, *37*, 2577–2601. [[CrossRef](#)]
17. Cao, S.; He, Y.; Zhang, L.; Chen, Y.; Yang, W.; Yao, S.; Sun, Q. Spatiotemporal Characteristics of Drought and Its Impact on Vegetation in the Vegetation Region of Northwest China. *Ecol. Indic.* **2021**, *133*, 108420. [[CrossRef](#)]
18. Zhang, Q.; Li, J.; Singh, V.P.; Bai, Y. SPI-Based Evaluation of Drought Events in Xinjiang, China. *Nat. Hazards* **2012**, *64*, 481–492. [[CrossRef](#)]
19. Sun, J.; Zhang, F. Daily Extreme Precipitation and Trends over China. *Sci. China Earth Sci.* **2017**, *60*, 2190–2203. [[CrossRef](#)]
20. Zhang, J.; Chen, H.; Zhang, Q. Extreme Drought in the Recent Two Decades in Northern China Resulting from Eurasian Warming. *Clim. Dyn.* **2019**, *52*, 2885–2902. [[CrossRef](#)]
21. Jiang, Y.; Wang, R.; Peng, Q.; Wu, X.; Ning, H.; Li, C. The Relationship between Drought Activity and Vegetation Cover in Northwest China from 1982 to 2013. *Nat. Hazards* **2018**, *92*, 145–163. [[CrossRef](#)]
22. Zhang, Q.; Yao, Y.; Wang, Y.; Wang, S.; Wang, J.; Yang, J.; Wang, J.; Li, Y.; Shang, J.; Li, W. Characteristics of Drought in Southern China under Climatic Warming, the Risk, and Countermeasures for Prevention and Control. *Theor. Appl. Climatol.* **2019**, *136*, 1157–1173. [[CrossRef](#)]
23. Chen, Y.; Zhao, Y.; Feng, J.; Wang, F. ENSO Cycle and Climate Anomaly in China. *Chin. J. Ocean. Limnol.* **2012**, *30*, 985–1000. [[CrossRef](#)]
24. Zhao, P.; Tan, L.; Zhang, P.; Wang, S.; Cui, B.; Li, D.; Xue, G.; Cheng, X. Stable Isotopic Characteristics and Influencing Factors in Precipitation in the Monsoon Marginal Region of Northern China. *Atmosphere* **2018**, *9*, 97. [[CrossRef](#)]
25. McKee, T.B.; Doesken, N.J.; Kleist, J. The Relationship of Drought Frequency and Duration to Time Scales. In Proceedings of the Eighth Conference on Applied Climatology, Anaheim, CA, USA, 17–22 January 1993; pp. 17–22.
26. Vicente-Serrano, S.M.; Beguería, S.; López-Moreno, J.I. A Multiscalar Drought Index Sensitive to Global Warming: The Standardized Precipitation Evapotranspiration Index. *J. Clim.* **2010**, *23*, 1696–1718. [[CrossRef](#)]
27. Palmer, W.C. *Meteorological Drought*; Research Paper, No. 45; U.S. Department of Commerce, Weather Bureau: Washington, DC, USA, 1965; p. 58.
28. Narasimhan, B.; Srinivasan, R. Development and Evaluation of Soil Moisture Deficit Index (SMDI) and Evapotranspiration Deficit Index (ETDI) for Agricultural Drought Monitoring. *Agric. For. Meteorol.* **2005**, *133*, 69–88. [[CrossRef](#)]
29. Liu, X.; Wang, S.; Zhou, Y.; Wang, F.; Li, W.; Liu, W. Regionalization and Spatiotemporal Variation of Drought in China Based on Standardized Precipitation Evapotranspiration Index (1961–2013). *Adv. Meteorol.* **2015**, *2015*, 950262. [[CrossRef](#)]
30. Alsafadi, K.; Al-Ansari, N.; Mokhtar, A.; Mohammed, S.; Elbeltagi, A.; Sh Sammen, S.; Bi, S. An Evapotranspiration Deficit-Based Drought Index to Detect Variability of Terrestrial Carbon Productivity in the Middle East. *Environ. Res. Lett.* **2022**, *17*, 014051. [[CrossRef](#)]
31. Hoffman, M.T.; Carrick, P.J.; Gillson, L.; West, A.G. Drought, Climate Change and Vegetation Response in the Succulent Karoo, South Africa. *S. Afr. J. Sci.* **2009**, *105*, 54. [[CrossRef](#)]
32. Tirivarombo, S.; Osupile, D.; Eliasson, P. Drought Monitoring and Analysis: Standardised Precipitation Evapotranspiration Index (SPEI) and Standardised Precipitation Index (SPI). *Phys. Chem. Earth Parts A/B/C* **2018**, *106*, 1–10. [[CrossRef](#)]
33. Li, L.; She, D.; Zheng, H.; Lin, P.; Yang, Z.-L. Elucidating Diverse Drought Characteristics from Two Meteorological Drought Indices (SPI and SPEI) in China. *J. Hydrometeorol.* **2020**, *21*, 1513–1530. [[CrossRef](#)]
34. Danandeh Mehr, A.; Vaheddoost, B. Identification of the Trends Associated with the SPI and SPEI Indices across Ankara, Turkey. *Theor. Appl. Clim.* **2020**, *139*, 1531–1542. [[CrossRef](#)]
35. Lee, S.-H.; Yoo, S.-H.; Choi, J.-Y.; Bae, S. Assessment of the Impact of Climate Change on Drought Characteristics in the Hwanghae Plain, North Korea Using Time Series SPI and SPEI: 1981–2100. *Water* **2017**, *9*, 579. [[CrossRef](#)]
36. Nedealcov, M.; Răileanu, V.; Sirbu, R.; Cojocari, R. The Use Of Standardized Indicators (SPI And SPEI) In Predicting Droughts Over The Republic Of Moldova Territory. *Present Environ. Sustain. Dev.* **2015**, *9*, 149–158. [[CrossRef](#)]
37. Mohammed, S.; Alsafadi, K.; Al-Awadhi, T.; Sherief, Y.; Harsanyie, E.; El Kenawy, A.M. Space and Time Variability of Meteorological Drought in Syria. *Acta Geophys.* **2020**, *68*, 1877–1898. [[CrossRef](#)]

38. Chaudhary, U.; Limbu, M.N.; Kaphle, G.C. Statistical Analysis of Rainfall Distribution in Biratnagar, Nepal: A Case Study. *Pragya Darshan* **2023**, *5*, 52–57. [[CrossRef](#)]
39. Liu, X.; Zhu, X.; Pan, Y.; Bai, J.; Li, S. Performance of Different Drought Indices for Agriculture Drought in the North China Plain. *J. Arid. Land* **2018**, *10*, 507–516. [[CrossRef](#)]
40. Mokhtar, A.; Jalali, M.; He, H.; Al-Ansari, N.; Elbeltagi, A.; Alsafadi, K.; Abdo, H.G.; Sammen, S.S.; Gyasi-Agyei, Y.; Rodrigo-Comino, J. Estimation of SPEI Meteorological Drought Using Machine Learning Algorithms. *IEEE Access* **2021**, *9*, 65503–65523. [[CrossRef](#)]
41. Yao, N.; Li, Y.; Lei, T.; Peng, L. Drought Evolution, Severity and Trends in Mainland China over 1961–2013. *Sci. Total Environ.* **2018**, *616–617*, 73–89. [[CrossRef](#)]
42. Xu, D.; Zhang, Q.; Ding, Y.; Zhang, D. Spatiotemporal Pattern Mining of Drought in the Last 40 Years in China Based on the SPEI and Space–Time Cube. *J. Appl. Meteorol. Climatol.* **2021**, *60*, 1219–1230. [[CrossRef](#)]
43. Li, J.; Hsu, H.-H.; Wang, W.-C.; Ha, K.-J.; Li, T.; Kitoh, A. East Asian Climate under Global Warming: Understanding and Projection. *Clim. Dyn.* **2018**, *51*, 3969–3972. [[CrossRef](#)]
44. Piao, S.; Ciais, P.; Huang, Y.; Shen, Z.; Peng, S.; Li, J.; Zhou, L.; Liu, H.; Ma, Y.; Ding, Y.; et al. The Impacts of Climate Change on Water Resources and Agriculture in China. *Nature* **2010**, *467*, 43–51. [[CrossRef](#)] [[PubMed](#)]
45. Schamm, K.; Ziese, M.; Becker, A.; Finger, P.; Meyer-Christoffer, A.; Schneider, U.; Schröder, M.; Stender, P. Global Gridded Precipitation over Land: A Description of the New GPCC First Guess Daily Product. *Earth Syst. Sci. Data* **2014**, *6*, 49–60. [[CrossRef](#)]
46. Harris, I.; Osborn, T.J.; Jones, P.; Lister, D. Version 4 of the CRU TS Monthly High-Resolution Gridded Multivariate Climate Dataset. *Sci. Data* **2020**, *7*, 109. [[CrossRef](#)]
47. Ali, R.; Kuriqi, A.; Abubaker, S.; Kisi, O. Long-Term Trends and Seasonality Detection of the Observed Flow in Yangtze River Using Mann-Kendall and Sen’s Innovative Trend Method. *Water* **2019**, *11*, 1855. [[CrossRef](#)]
48. Kendall, M.G. *Rank Correlation Methods*, 4th ed.; Charles Griffin: London, UK, 1975.
49. Mann, H.B. Nonparametric Tests Against Trend. *Econometrica* **1945**, *13*, 245. [[CrossRef](#)]
50. Sanogo, A.; Kabange, R.S.; Owusu, P.A.; Djire, B.I.; Donkoh, R.F.; Dia, N. Investigation into Recent Temperature and Rainfall Trends in Mali Using Mann-Kendall Trend Test: Case Study of Bamako. *GEP* **2023**, *11*, 155–172. [[CrossRef](#)]
51. Neeti, N.; Eastman, J.R. A Contextual Mann-Kendall Approach for the Assessment of Trend Significance in Image Time Series: A Novel Method for Testing Trend Significance. *Trans. GIS* **2011**, *15*, 599–611. [[CrossRef](#)]
52. Hamed, K.H.; Ramachandra Rao, A. A Modified Mann-Kendall Trend Test for Autocorrelated Data. *J. Hydrol.* **1998**, *204*, 182–196. [[CrossRef](#)]
53. Theil, H. A Rank-Invariant Method of Linear and Polynomial Regression Analysis. In *Henri Theil’s Contributions to Economics and Econometrics*; Raj, B., Koerts, J., Eds.; Advanced Studies in Theoretical and Applied Econometrics; Springer: Dordrecht, The Netherlands, 1992; Volume 23, pp. 345–381. ISBN 978-94-010-5124-8.
54. Sen, P.K. Estimates of the Regression Coefficient Based on Kendall’s Tau. *J. Am. Stat. Assoc.* **1968**, *63*, 1379–1389. [[CrossRef](#)]
55. Yevjevich, V. An Objective Approach to Definitions and Investigations of Continental Hydrologic Droughts. *J. Hydrol.* **1967**, *7*, 353. [[CrossRef](#)]
56. Zhang, L.; Xiao, J.; Zhou, Y.; Zheng, Y.; Li, J.; Xiao, H. Drought Events and Their Effects on Vegetation Productivity in China. *Ecosphere* **2016**, *7*, e01591. [[CrossRef](#)]
57. Alsafadi, K.; Mohammed, S.A.; Ayugi, B.; Sharaf, M.; Harsányi, E. Spatial–Temporal Evolution of Drought Characteristics Over Hungary Between 1961 and 2010. *Pure Appl. Geophys.* **2020**, *177*, 3961–3978. [[CrossRef](#)]
58. Moran, P.A.P. The Interpretation of Statistical Maps. *J. R. Stat. Soc. Ser. B* **1948**, *10*, 243–251. [[CrossRef](#)]
59. Assuncao, R.M.; Reis, E.A. A new proposal to adjust Moran’s I for population density. *Stat. Med.* **1999**, *18*, 2147. [[CrossRef](#)]
60. Anselin, L. Local Indicators of Spatial Association–LISA. *Geogr. Anal.* **2010**, *27*, 93–115. [[CrossRef](#)]
61. Anselin, L.; Syabri, I.; Kho, Y. GeoDa: An Introduction to Spatial Data Analysis. *Geogr. Anal.* **2006**, *38*, 5–22. [[CrossRef](#)]
62. Chen, M.; Gong, Y.; Li, Y.; Lu, D.; Zhang, H. Population Distribution and Urbanization on Both Sides of the Hu Huanyong Line: Answering the Premier’s Question. *J. Geogr. Sci.* **2016**, *26*, 1593–1610. [[CrossRef](#)]
63. Liu, J.; Yang, Q.; Liu, J.; Zhang, Y.; Jiang, X.; Yang, Y. Study on the Spatial Differentiation of the Populations on Both Sides of the “Qinling-Huaihe Line” in China. *Sustainability* **2020**, *12*, 4545. [[CrossRef](#)]
64. Yang, J.; Yang, Y.; Li, Z.; Liao, L.; Gan, R.; Wang, W.; Wang, T.; Liang, L. The Regional Characteristics of Meteorological Drought Event and Its Multidimensional Factors Measurement by Daily SPEI in Guangxi, China. *Geomat. Nat. Hazards Risk* **2023**, *14*, 117–142. [[CrossRef](#)]
65. Tan, C.; Yang, J.; Li, M. Temporal-Spatial Variation of Drought Indicated by SPI and SPEI in Ningxia Hui Autonomous Region, China. *Atmosphere* **2015**, *6*, 1399–1421. [[CrossRef](#)]
66. Mohammed, S.; Alsafadi, K.; Enaruvbe, G.O.; Bashir, B.; Elbeltagi, A.; Széles, A.; Alsalman, A.; Harsanyi, E. Assessing the Impacts of Agricultural Drought (SPI/SPEI) on Maize and Wheat Yields across Hungary. *Sci. Rep.* **2022**, *12*, 8838. [[CrossRef](#)] [[PubMed](#)]
67. Feng, W.; Lu, H.; Yao, T.; Yu, Q. Drought Characteristics and Its Elevation Dependence in the Qinghai–Tibet Plateau during the Last Half-Century. *Sci. Rep.* **2020**, *10*, 14323. [[CrossRef](#)] [[PubMed](#)]
68. Wang, R.; Chen, J.; Chen, X.; Wang, Y. Variability of Precipitation Extremes and Dryness/Wetness over the Southeast Coastal Region of China, 1960–2014. *Int. J. Climatol.* **2017**, *37*, 4656–4669. [[CrossRef](#)]

69. Li, H.; Hou, E.; Deng, J. Spatio-Temporal Differentiation Characteristic and Evolution Process of Meteorological Drought in Northwest China From 1960 to 2018. *Front. Earth Sci.* **2022**, *10*, 857953. [[CrossRef](#)]
70. Yao, J.; Zhao, Y.; Chen, Y.; Yu, X.; Zhang, R. Multi-Scale Assessments of Droughts: A Case Study in Xinjiang, China. *Sci. Total Environ.* **2018**, *630*, 444–452. [[CrossRef](#)]
71. Wan, H.; Zhong, Z.; Yang, X.; Li, X. Impact of City Belt in Yangtze River Delta in China on a Precipitation Process in Summer: A Case Study. *Atmos. Res.* **2013**, *125–126*, 63–75. [[CrossRef](#)]
72. Liu, J.; Schlünzen, K.H.; Frisius, T.; Tian, Z. Effects of Urbanization on Precipitation in Beijing. *Phys. Chem. Earth Parts ABC* **2021**, *122*, 103005. [[CrossRef](#)]
73. Liu, K.; Li, X.; Wang, S.; Li, Y. Investigating the Impacts of Driving Factors on Urban Heat Islands in Southern China from 2003 to 2015. *J. Clean. Prod.* **2020**, *254*, 120141. [[CrossRef](#)]
74. Ma, F.; Yuan, X. More Persistent Summer Compound Hot Extremes Caused by Global Urbanization. *Geophys. Res. Lett.* **2021**, *48*, e2021GL093721. [[CrossRef](#)]
75. Gao, Z.; Zhu, J.; Guo, Y.; Luo, N.; Fu, Y.; Wang, T. Impact of Land Surface Processes on a Record-Breaking Rainfall Event on May 06–07, 2017, in Guangzhou, China. *Geophys. Res. Atmos.* **2021**, *126*, e2020JD032997. [[CrossRef](#)]
76. Lorenz, J.M.; Kronenberg, R.; Bernhofer, C.; Niyogi, D. Urban Rainfall Modification: Observational Climatology Over Berlin, Germany. *J. Geophys. Res. Atmos.* **2019**, *124*, 731–746. [[CrossRef](#)]
77. Luo, M.; Lau, N. Increasing Heat Stress in Urban Areas of Eastern China: Acceleration by Urbanization. *Geophys. Res. Lett.* **2018**, *45*, 13060–13069. [[CrossRef](#)]
78. Yang, X.; Zhang, L.; Wang, Y.; Singh, V.P.; Xu, C.-Y.; Ren, L.; Zhang, M.; Liu, Y.; Jiang, S.; Yuan, F. Spatial and Temporal Characterization of Drought Events in China Using the Severity-Area-Duration Method. *Water* **2020**, *12*, 230. [[CrossRef](#)]
79. Han, R.; Li, Z.; Li, Z.; Han, Y. Spatial–Temporal Assessment of Historical and Future Meteorological Droughts in China. *Atmosphere* **2021**, *12*, 787. [[CrossRef](#)]
80. Yue, Y.; Liu, H.; Mu, X.; Qin, M.; Wang, T.; Wang, Q.; Yan, Y. Spatial and Temporal Characteristics of Drought and Its Correlation with Climate Indices in Northeast China. *PLoS ONE* **2021**, *16*, e0259774. [[CrossRef](#)]
81. McGregor, G.R.; Ebi, K. El Niño Southern Oscillation (ENSO) and Health: An Overview for Climate and Health Researchers. *Atmosphere* **2018**, *9*, 282. [[CrossRef](#)]
82. Zhang, L.; Wu, P.; Zhou, T.; Xiao, C. ENSO transition from La Niña to El Niño drives prolonged spring–summer drought over North China. *J. Clim.* **2018**, *31*, 3509–3523. [[CrossRef](#)]
83. Zhang, W.; Jin, F.-F.; Turner, A. Increasing Autumn Drought over Southern China Associated with ENSO Regime Shift. *Geophys. Res. Lett.* **2014**, *41*, 4020–4026. [[CrossRef](#)]
84. Deng, S.; Chen, T.; Yang, N.; Qu, L.; Li, M.; Chen, D. Spatial and Temporal Distribution of Rainfall and Drought Characteristics across the Pearl River Basin. *Sci. Total Environ.* **2018**, *619–620*, 28–41. [[CrossRef](#)]
85. Cui, K.; Shoemaker, S.P. A Look at Food Security in China. *Npj Sci. Food* **2018**, *2*, 4. [[CrossRef](#)]
86. Qin, Z.; Tang, H.; Li, W.; Zhang, H.; Zhao, S.; Wang, Q. Modelling Impact of Agro-Drought on Grain Production in China. *Int. J. Disaster Risk Reduct.* **2014**, *7*, 109–121. [[CrossRef](#)]
87. Yu, C.; Huang, X.; Chen, H.; Huang, G.; Ni, S.; Wright, J.S.; Hall, J.; Ciais, P.; Zhang, J.; Xiao, Y.; et al. Assessing the Impacts of Extreme Agricultural Droughts in China Under Climate and Socioeconomic Changes. *Earths Future* **2018**, *6*, 689–703. [[CrossRef](#)]
88. Pei, W.; Fu, Q.; Liu, D.; Li, T.; Cheng, K.; Cui, S. Spatiotemporal Analysis of the Agricultural Drought Risk in Heilongjiang Province, China. *Theor. Appl. Clim.* **2018**, *133*, 151–164. [[CrossRef](#)]
89. Lei, Y.; Wang, J.; Yue, Y.; Yin, Y.; Sheng, Z. How Adjustments in Land Use Patterns Contribute to Drought Risk Adaptation in a Changing Climate—A Case Study in China. *Land. Use Policy* **2014**, *36*, 577–584. [[CrossRef](#)]
90. Huang, J.; Xue, Y.; Sun, S.; Zhang, J. Spatial and Temporal Variability of Drought during 1960–2012 in Inner Mongolia, North China. *Quat. Int.* **2015**, *355*, 134–144. [[CrossRef](#)]

Disclaimer/Publisher’s Note: The statements, opinions and data contained in all publications are solely those of the individual author(s) and contributor(s) and not of MDPI and/or the editor(s). MDPI and/or the editor(s) disclaim responsibility for any injury to people or property resulting from any ideas, methods, instructions or products referred to in the content.